2020 IEEE International Conference on Robotics and Automation (ICRA)
31 May - 31 August, 2020. Paris, France

Safe high impedance control of a series-elastic actuator with a disturbance observer

Kevin Haninger[1], Abner Asignacion[2], Sehoon Oh[2]

***Abstract*—In many series-elastic actuator applications, the ability to safely render a wide range of impedance is important. Advanced torque control techniques such as the disturbance observer (DOB) can improve torque tracking performance, but their impact on safe impedance range is not established. Here, safety is defined with load port passivity, and passivity conditions are developed for two variants of DOB torque control. These conditions are used to determine the maximum safe stiffness and Z-region of the DOB controllers, which are analyzed and compared with the no DOB case. A feedforward controller is proposed which increases the maximum safe stiffness of the DOB approaches. The results are experimentally validated by manual excitation and in a high-stiffness environment.**

I. Introduction

Torque control of series-elastic actuators (SEAs) [1] brings them closer to ideal torque sources, supporting higher-level control such as impedance control [2]. Torque control performance, in the sense of torque tracking bandwidth and disturbance rejection, can be improved with high-gain control, commonly realized with PID or the disturbance observer (DOB) [3], [4]. However, the torque controller should also support other senses of performance, such as the safe rendering of a wide range of impedance. Realizing a high impedance can be useful in applications which require motion control performance [5], while a physical compliance allows the system to retain good collision performance [6], [7].

To measure the range of impedance, the Z-width can be used [8], which measures the range of impedance parameters which are 'achievable'. Recent work has shown that high-gain torque control reduces the Z-width of an actuator on hydraulic [9] and electric actuators [10], raising questions about the use of high-gain torque control. However, the impedance control parameters do not directly correspond to the rendered impedance at the interaction port, and the difference can be significant if the inner-loop control has poor tracking performance (i.e. low gain inner-loop control). An alternative metric is the Z-region [11], which is 'the achievable magnitude range (width) over a frequency range (depth)'. Both of these metrics require a realistic means of determining the impedance limits. These limits are typically due to safety constraints, which can be found experimentally [8], but for design and analysis a practical model-based condition is needed.

[1] Affiliated with the Division of Automation Technology, Fraunhofer Institute for Production Systems and Design Technology (IPK), Berlin, Germany (kevin.haninger@ipk.fraunhofer.de
[2] Affiliated with the Department of Robotic Engineering, Daegu Gyeongbuk Institute of Science and Technology, Daegu, Korea

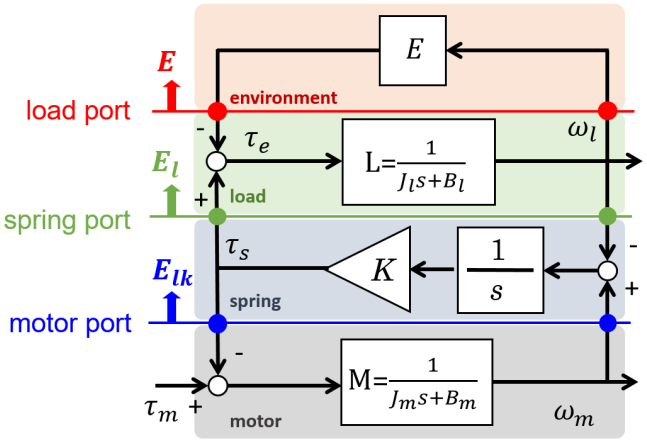

Fig. 1: Schematic for an SEA integrated to an application, with motor dynamics M coupled to load dynamics L through the elastic element K. The passive environment E couples to the load dynamics. Three power-continuous interaction ports are shown.

Safety for interactive robots is classically shown with passivity, which guarantees coupled stability with an arbitrary (strictly) passive environment [2]. This has been used as a design condition for hierarchical control of SEAs with: torque/velocity control [12], impedance/torque/velocity control [13], [14], and in comparative studies [15], [16]. Analysis based on passivity has established the importance of motor damping and torque control derivative action [17], [13]. However, passivity conditions for DOB torque control are not established. Many of the stability proofs for DOB torque control assume bounded parametric uncertainty, raising questions about stability in arbitrary environments.

Passivity does not perfectly correspond to practical safety. The conservatism of passivity is well-known [18], [19], and various passivity relaxations have been proposed, including analyzing passivity at different ports [20] and replacing passivity with a mixed passivity/small-gain condition [21]. Passivity observers have also been implemented on SEAs [22], [20], enforcing passivity by modifying the control signal, albeit at the cost of complexity and performance. Here, passivity at the load port is used as a design condition, instead of the spring port.

The DOB is used in many state-of-the-art SEA controllers, including rotary [4], [23], [24], linear [25], cable-driven [26],

978-1-7281-7395-5/20/$31.00 ©2020 IEEE

NOMENCLATURE

Dynamics	M	Motor dynamics
	K	Spring
	L	Load dynamics
	N	Inverse gear ratio
Control	I	Impedance control
		I_u, maximum passive impedance
	C	PD Feedback control
	C_{ff}	Feedforward control
	Q	DOB tuning filter
	P_m	Plant model used in DOBm
	P_t	Plant model used in DOBt

and multiple-stiffness [27] SEAs. Performance is typically shown by the reference tracking bandwidth and disturbance rejection of the torque loop. Outer-loop position control on an SEA with a DOB has also been established [25], [27]. Impedance control with an inner-loop DOB is also established [23], where the DOB is shown to reduce the need for high-gain PID torque feedback control. However, the ability to render high impedances with a DOB, especially such that safety is maintained in high-stiffness environments, is not yet investigated.

To investigate high impedance rendering with DOB torque control, two DOB architectures are considered in this paper, the first closed around the motor dynamics [4], and the second closed around the torque dynamics [24]; referred to as DOBm and DOBt respectively. To evaluate the safe impedance range realistically, this paper develops safety conditions based on passivity at the load port for both DOBs and PD torque control. These conditions motivate the maximum safe stiffness and the limits of the Z-region. The Z-region and maximum safe stiffness are analyzed, and feedforward controllers are proposed for the DOBm and DOBt which increase the maximum safe stiffness. Experimental validation demonstrates coupled stability in a high stiffness environment, and load port passivity under manual excitation is also shown.

II. Control Architecture and Metrics

This section reviews the DOB for SEA control, as well as safety and performance metrics which will be considered.

A. Disturbance Observer

The disturbance observer is a frequency-domain control technique often used in precision motion control [3], which uses the inverse of a nominal plant model to estimate external disturbances, then adds the inverse of the estimated disturbance to the control input for cancellation. In addition to the rejection of disturbances, the DOB enforces nominal dynamics, making the plant appear as the nominal model within the Q-filter bandwidth, improving the accuracy of feed-forward compensators [28].

In applying the DOB to SEAs, the DOB is typically applied around the motor dynamics [4], but recent work has shown advantages in applying the DOB to the torque output [24]. Denoting these DOBm and DOBt (respectively), their block diagram can be seen in Figure 2. The spring port dynamics which result can be seen in Table I.

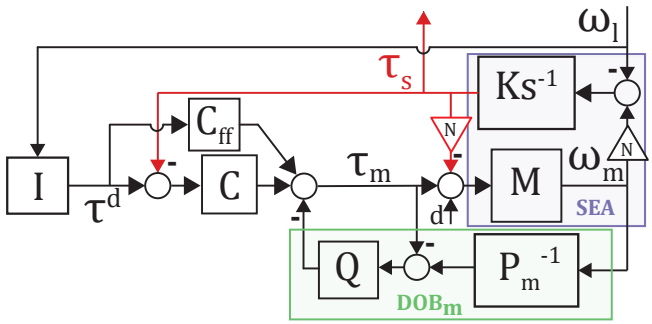

(a) DOBm

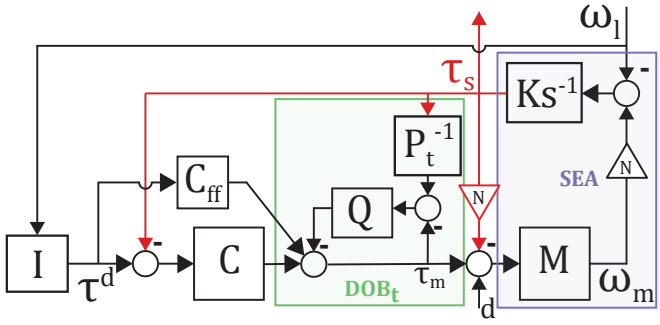

(b) DOBt

Fig. 2: Two DOB architectures for SEAs, where the DOB is closed around (a) motor dynamics and (b) torque dynamics. The DOB consists of the inverse of models P_m and P_t and tuning filter Q. The impedance controller I determines reference torque τ^d. Feedback C and feedforward control C_{ff} complete the inner control. Inverse gear ratio N relates motor dynamics M to the spring K. Additional signals are disturbance d, load velocity ω_l, motor velocity ω_m, spring torque τ_s, and motor torque τ_m.

The inverse models used in the DOBm and DOBt are the nominal models of the effective plant of the DOB loop under fixed output, $P_m = \hat{M}$ and $P_t = \hat{M}(1 + \hat{M}Ks^{-1})^{-1}$, where $\hat{M}$ is the model for motor dynamics M. Second-order low-pass filters are used for Q filters, with cutoff frequency ω_{D}, $Q(s) = \omega_{\mathrm{D}}^2(s^2 + 1.4142\omega_{\mathrm{D}}s + \omega_{\mathrm{D}}^2)^{-1}$.

B. Coupled stability

To analyze the coupled stability of the SEA with an arbitrary passive environment, the SEA and environment can be separated at any of the ports shown in Figure 1. Often, the passivity of the SEA at the spring port is investigated [12], [14], while other work has investigated passivity at the load port [29], [20], [13]. The load dynamics are the dynamics of the mechanism permanently attached to the output of the SEA, which are typically known. The dynamics rendered at the spring port can be seen in Table I, the load dynamics can be written as

$$\frac{\omega_l}{\tau_e} = \frac{L}{1 + LZ_s}, \tag{1}$$

where Z_s is the spring port dynamics (from ω_l to τ_s), as specified in Table I.

C. Performance metrics

The typical design metric for torque control is torque tracking bandwidth with a fixed output position (i.e. infinite environmental stiffness). Although useful for comparison, its generalization to lower impedance environments or to different application requirements (e.g. large Z-region) is unclear. The performance of impedance control can be characterized by the accuracy of the rendered impedance [30], but in many applications the range of impedance which can be rendered is more important than the accuracy.

1) Z-region: Z-width [8] is the range of impedance parameters which can be achieved, originally proposed on haptic systems. For SEAs, where inner-loop control is typical, the impedance parameters do not directly correspond to port dynamics - they also depend on the performance of the torque control. To address this, Z-region is proposed [11], which measures the range in impedance which can be rendered at the interaction port - the area between the maximum and minimum impedance magnitude in the frequency domain. Given the port dynamics at the upper and lower impedance limits $Z_u(s)$ and $Z_l(s)$, a weighting filter $W(\omega)$, and frequency band of interest $[\omega_1, \omega_2]$, the metric is defined as

$$Z_{region} = \int_{\omega_1}^{\omega_2} W(\omega) \left| \ln |Z_u(j\omega)| - \ln |Z_l(j\omega)| \right| d\omega.$$

Here, to simplify, the weighting filter is taken as unity ($W(\omega) = 1$) and Z_l is taken as the zero-impedance control $I(s) = 0$ (zero-impedance control rarely has stability problems). The complete frequency domain is considered, giving:

$$Z_{region} = \int_0^{\infty} \left| \ln \left| \frac{Z_u(j\omega)}{Z_l(j\omega)} \right| \right| d\omega. \tag{2}$$

The resulting expressions for the controllers considered here can be seen in Table I.

2) Maximum rendered stiffness: In addition to Z-region, the rendered stiffness is considered. These expressions can be derived by taking the limit of spring port dynamics as $\omega \to 0$, and are seen in the right column of Table I.

D. Performance with coupled stability

To consider the real-world achievable performance, a realistic coupled stability constraint must be considered. A coupled stability condition is spring port passivity - i.e. the positive-realness of $\omega_l \to \tau_s = Z_s$. Designing the controllers to maximize safe rendered stiffness is then

$$\max_{K_{imp},C,C_{ff},Q} \lim_{\omega \to 0} |\omega Z_s(j\omega)| \quad \text{s.t.} \quad \mathtt{Re}(Z_s) > 0. \tag{3}$$

When the spring port passivity is the safety constraint, the maximum rendered stiffness is K, the physical stiffness [31]. As outlined in Section II-B, the passivity at the load port can be used as an alternative [29]. Maximizing rendered stiffness under the load port passivity constraint can be written as

$$\max_{K_{imp},C,C_{ff},Q} \lim_{\omega \to 0} |\omega Z_s| \quad \text{s.t.} \quad \mathtt{Re}\{\frac{L}{1+LZ_s}\} > 0 \tag{4}$$

$$\max_{K_{imp},C,C_{ff},Q} \lim_{\omega \to 0} |\omega Z_s| \quad \text{s.t.} \quad s\mathtt{Re}\{Z_l\} > B_l \tag{5}$$

where (5) is found by inverting the load port dynamics, and noting that only the B_l term in the load dynamics is real.

To write the passivity constraint in terms of parameters, take the plant model seen in Figure 1, where J_m, J_l and B_m, B_l are the inertia and damping of the motor and load respectively. The controller C is taken as a PD controller, $C = K_p + K_d s$. The load passivity can be written in closed form (with the aid of a symbolic algebra system), for the no DOB case giving

$$\begin{aligned}
\mathtt{Re}\{Z_l\} &= \frac{c_4\omega^4 + c_2\omega^2 + c_0}{KN(J_m K_d \omega^2 - KK_d N^2 + B_m K_p)} \\
c_4 &= B_l J_m \\
c_2 &= B_l B_m + 2B_l B_m K K_d N + J_m K_d K^2 N \cdots \\
&\quad -2B_l J_m K N(K_p + 1) + B_l K_d^2 K^2 N^2 \\
c_0 &= K^2 N(B_m K_p + B_m N + B_l K_p^2 N) \cdots \\
&\quad +K^2 N(2B_l K_p N^2 + B_l N^3)
\end{aligned} \tag{6}$$

While these conditions are not obviously convex or otherwise computationally tractable, they are analyzed empirically for controller design in the next section.

III. Controller Architecture and Design

This section presents analysis and design for high-stiffness DOB-based SEA control. Parameter settings for high-impedance rendering are motivated, as well as a feedforward compensation which improves the safe high-impedance limit.

A. Architecture comparison

From the maximum stiffness expressions in Table I, the DOB architectures allow improved rejection of disturbance torques d (i.e. friction in backdriveability) when $|Q| \to 1$ (i.e. at low frequencies). This allows the DOB to achieve the same accuracy of rendered stiffness (i.e. $\tau_s = K_{imp}\theta_l$) with a lower magnitude feedback control $|C|$, as established in [23].

In the Z-region analysis, note that $\mathtt{Re}(M(C+C_{ff})I_u) > 0$ $\forall\omega$for PD torque control and typical motor/impedance models. Thus, for a fixed I_u, increasing $|C|$ increases the Z-region. While other work has shown increasing $|C|$ decreases Z-*width* [10], the Z-*region* increases with $|C|$ for these three control architectures. For the DOBt, if $\mathtt{Re}(M(C+C_{ff}I_u(1-Q)^{-1}) > 0$ $\forall\omega$ (met on the system parameters used here), as $|Q| \to 1$, the Z-region increases. Thus, for the DOBt, increasing the bandwidth of the Q-filter theoretically improves the Z-region.

B. Analysis of feedback control

Here, the performance of the $\mathrm{DOB_m}$ and $\mathrm{DOB_t}$ are compared to the no DOB case. Feedforward control C_{ff} is set to the feedforward proposed in each of the original implementations, $C_{ff} = 0$ and $C_{ff} = P_t^{-1}Q$, for the DOBm and DOBt respectively. The maximum safe stiffness is found by taking

	Spring port dynamics	Z-region	Rendered stiffness
DOBm	$\tau_s = \frac{Ks^{-1}\left(N\tilde{M}\left(C+C_{ff}\right)I+1\right)\omega_l+Ks^{-1}\tilde{M}(1-Q)Nd}{1+Ks^{-1}N\tilde{M}(C+N(1-Q))}$	$\int_0^\infty \ln\left\lvert N\tilde{M}\left(C+C_{ff}\right)I_u+1\right\rvert d\omega$	$\tau_s\lvert_{\omega=0} = \frac{\left(K_p+C_{ff}\right)K_{imp}\theta_l+(1-Q)d}{\left(K_p+1-Q\right)}$
DOBt	$\tau_s = \frac{Ks^{-1}\left(NM\left(C+C_{ff}\right)I+1-Q\right)\omega_l+Ks^{-1}M(1-Q)Nd}{1-Q+QMP_t^{-1}+Ks^{-1}NM\left(C+N(1-Q)+QMP_t^{-1}\right)}$	$\int_0^\infty \ln\left\lvert N\frac{M\left(C+C_{ff}\right)I_u}{1-Q}+1\right\rvert d\omega$	$\tau_s\lvert_{\omega=0} = \frac{\left(K_p+C_{ff}\right)K_{imp}\theta_l+(1-Q)d}{\left(K_p+1-Q+QMP_t^{-1}\right)}$
No DOB	$\tau_s = \frac{Ks^{-1}\left(NM\left(C+C_{ff}\right)I+1\right)\omega_l+Ks^{-1}MNd}{1+Ks^{-1}NM(C+N)}$	$\int_0^\infty \ln\left\lvert NM\left(C+C_{ff}\right)I_u+1\right\rvert d\omega$	$\tau_s\lvert_{\omega=0} = \frac{\left(K_p+C_{ff}\right)K_{imp}\theta_l+d}{\left(K_p+1\right)}$

TABLE I: Spring port dynamics and performance metrics of the three controllers on a two-inertia SEA model, with dynamics as defined in Figure 2, where $M = \hat{M}(1+\Delta)$, $\tilde{M} = M(1-Q\Delta)^{-1}$, and $\theta_l = \omega_l s^{-1}$. I_u denotes the maximum passive impedance.

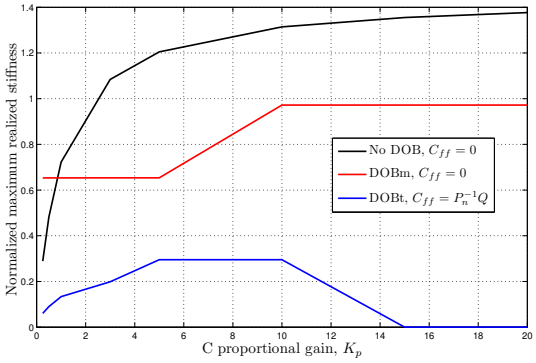

Fig. 3: Normalized realized stiffness $K^{-1}\frac{\tau_s}{\omega_l}\lvert_{\omega=0}$ vs. feedback gain K_p. The maximum stiffness is as defined by (4) with the C_{ff} proposed in the original DOBm and DOBt.

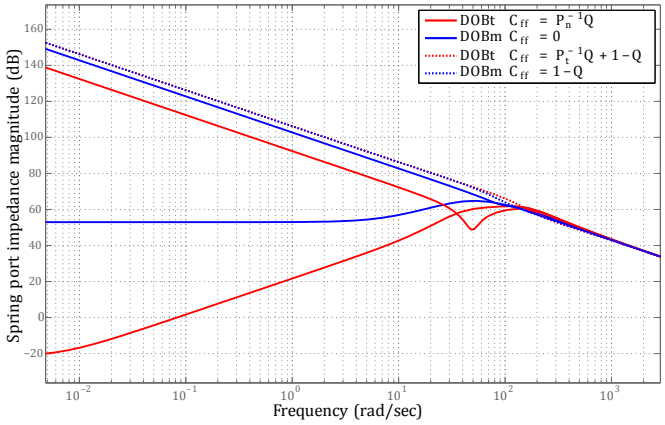

Fig. 4: Boundaries of the Z-region of DOBm and DOBt under various C_{ff}. The feedforward compensation proposed in (7) improves the Z-region, and is especially important for the DOBt. Note the low-impedance performance for DOBm and DOBt is unchanged by feedforward control. The no DOB with feedforward $C_{ff} = 1$ matches the DOBm with feedforward, and is therefore not shown.

$I = K_{imp}$ and incrementally increasing K_{imp} until (6) (and similar conditions for the DOB cases) is violated.

The impact of proportional feedback K_p on maximum rendered stiffness can be seen in Figure 3, showing that while it monotonically improves maximum stiffness for the no DOB and DOBm, the DOBt benefits more from a moderate K_p value. For other parameters, the results are monotonic and therefore not shown graphically: increasing the Q filter cutoff frequency ω_D or derivative feedback K_d increases maximum safe stiffness. Increasing B_{imp} does not make a large impact, and is thus left at $B_{imp} = 0$ in the maximum stiffness experiments to reduce noise.

C. Feedforward control

To motivate an improved C_{ff} for the DOBm and DOBt, compensators are proposed to match terms in the torque port dynamics, most easily seen in the rendered stiffness in Table I.

$$C_{ff} = \begin{cases} N(1-Q) & \text{DOBm} \\ P_t^{-1}Q + N(1-Q) & \text{DOBt} \end{cases} \tag{7}$$

When the steady-state magnitude of Q is slightly less than one, $1-Q$ acts as a lead filter, advancing the phase of the system, improving the phase at the load port.

The impact of these feedforward compensators on the Z-region can be seen in Figure 4. The baseline feedforward compensators are those used in the initial proposals of these controllers. The upper impedance is defined with load port passivity, and the lower limit is the zero impedance case $I = 0$. It can be seen that the feedforward compensator increase the maximum safe impedance, especially for the DOBt. Additionally, the lower impedance limit of the DOBt is substantially lower than that of the DOBm. The no DOB controller is the same as the DOBm with feedforward, so is not shown.

IV. Experimental Validation

A. Experimental setup

To verify the proposed approaches, a reaction force series elastic actuator (RFSEA) is used, as shown in Figure 5. It consists of Brushless DC motor (Maxon EC 4-pole 305015) with a maximum continuous torque of 92.9mNm. The motor is equipped with an incremental encoder before the gearbox, while the spring deflection is obtained by the high-resolution rotary incremental encoder. The physical parameters of the RFSEA are identified by using the FFT analyzer (ONO-SOKKI, CF-9400). In various load conditions, the sweep sine signals were applied to the RFSEA, and the motor velocity and

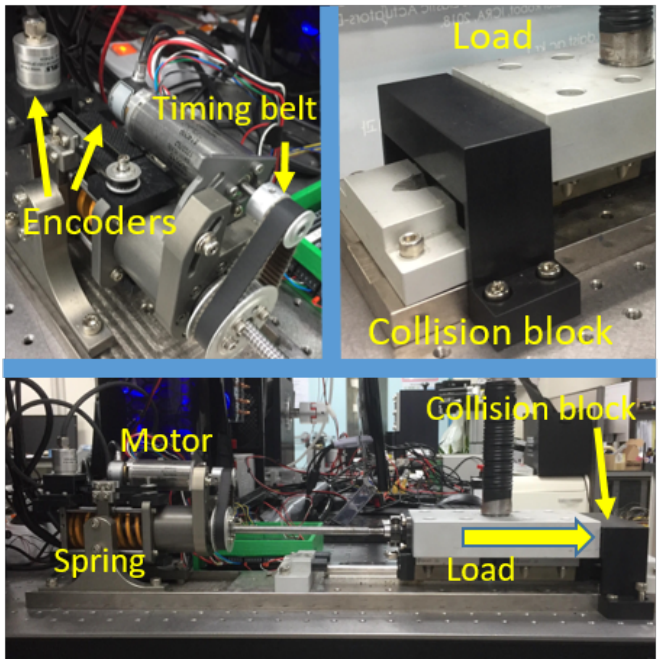

Fig. 5: Experimental setup used in validating the real-world coupled stability of the SEA.

the spring deformation were measured using encoders. Then, the parameters shown in Table IV were identified.

B. Coupled stability validation

To investigate if passivity corresponds well to real-world coupled stability, experiments were done with two high-stiffness environments, a rubber and metal block. A step input was given to the impedance controller while in contact with the two environments. The load arrow in Figure 5 shows the direction of the collision and reference direction for the fixed load condition. Controller parameters were varied in the ranges $K_p = [1, \dots 10]$,$K_d = [0.01, \dots, .1]$, $\omega_{\mathrm{D}}(hz) = [10, \dots, 100]$ under an outer-loop impedance of $I = K_{imp}s^{-1} + B_{imp}$ with $K_{imp} = 1000$ and $B_{imp} = 0.1$.

Each case is marked stable or unstable, with an experiment repeated if marginal stability (sustained oscillation) resulted. Trials with growing oscillation or a diverging load position are marked as unstable, otherwise coupled stable. A total of 80 cases were tried, where 7 are unstable. The load and spring port passivity were checked based on (6) (and similar for the DOB cases) for each set of gains. The false positives or negatives are reported, based on whether load/spring passivity predicts experimental coupled stability.

The zero-impedance case $I = 0$ (i.e. torque control) was also checked for instability, where higher PD controller gains typically result in motor failure (e.g. motor overheat) rather than instability. In pure torque control, it is difficult to obtain instability even in impact scenarios.

	DOBm		DOBt	
	# FP	# FN	# FP	# FN
Spring Port Passivity	0	12	0	15
Load Port Passivity	0	0	1	0

TABLE II: Experiments are conducted over eighty different controller settings, and passivity at the spring and load port checked. FP = False Positive, condition true but system not experimentally stable (ideally 0). FN = False Negative, condition false but system experimentally stable (conservatism, ideally 0).

The experimental results are shown in Table II, and demonstrate the conservatism of the spring port passivity condition, with 12 and 15 false negatives for DOBm and DOBt. For the DOBm, high K_p and B_{imp} caused instability, and decreasing K_{imp} did not restore coupled stability when there is a high K_p or B_{imp}. The DOBt allows higher K_p and K_d gain values than the DOBm, but it is unstable with higher values of B_{imp} or K_d. For instance, with the DOBm, B_{imp} can go as high as 50 with coupled stability, but for the DOBt, B_{imp} is limited to values less than 1 (on this experimental setup).

C. Maximum rendered stiffness validation

Experimentally determining the maximum impedance stiffness K_{imp} that can be safely rendered is done by finding the maximum stiffness where load port passivity is held for the no DOB, DOBm, and DOBt architectures. In these experiments, a high-stiffness hammer is used to strike the load side, where a load cell measures the external force τ_e. This allows evaluation of load port passivity using a passivity observer, which measures the instantaneous port power flow from the product of ω_l and τ_e, which can then be integrated over time for total energy flow. The results, shown in Figure 6, indicate decreasing energy as a passivity violation at the load port. Controller gains of $B_{imp} = 0$, $K_d = .01$ and $\omega_{\mathrm{D}} = 25$ Hz are used, as motivated in the Section III-B.

	Spring pass.	Load pass.	Experiment
No DOB	1	1.93	~ 1.7
DOBm	1	1.93	~ 1.8
DOBt	1	1.85	~ 1.65

TABLE III: The maximum normalized stiffness K_{imp}/K achieved from numerical analysis with spring and load passivity, and compared with the achieved experimental results. The load port passivity predicts maximum stiffness more closely, and the DOBm allows for a slightly higher high stiffness than the DOBt and no DOB experimentally.

Table III supports the following points: (i) K_{imp} can be safely set higher than K; (ii) the load port condition gives a less conservative, more practical limit for K_{imp}, (iii) DOBm realizes the highest stiffness experimentally, which is not predicted analytically. However, the lower performance of the DOBt is predicted. The difference between the simulation and

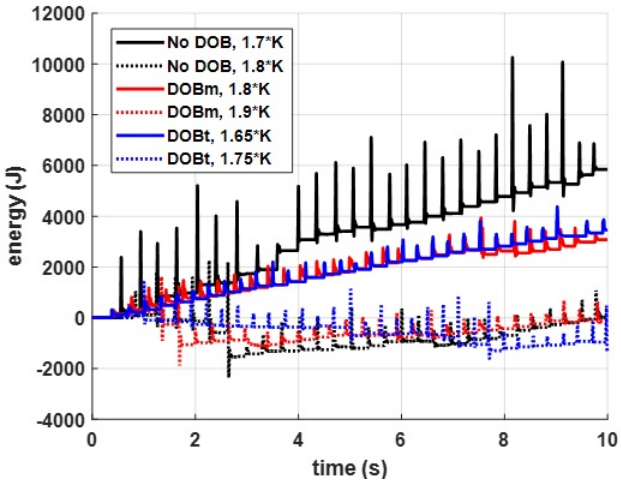

Fig. 6: Passivity at the load-port for high stiffnesses K_{imp}. The experimental passive stiffness limit lies between the two K_{imp} values for each architecture, as the solid lines indicate passive behavior, dotted not passive.

J_m	$6.4e-6$ kg $\cdot$ m^2	J_l	7 kg $\cdot$ m^2
B_m	$6e-5$ Nm $\cdot$ s/rad	B_l	100 Nm $\cdot$ s/rad
K	141350 N/m	N	1/7854 rad/m

TABLE IV: Identified Parameters

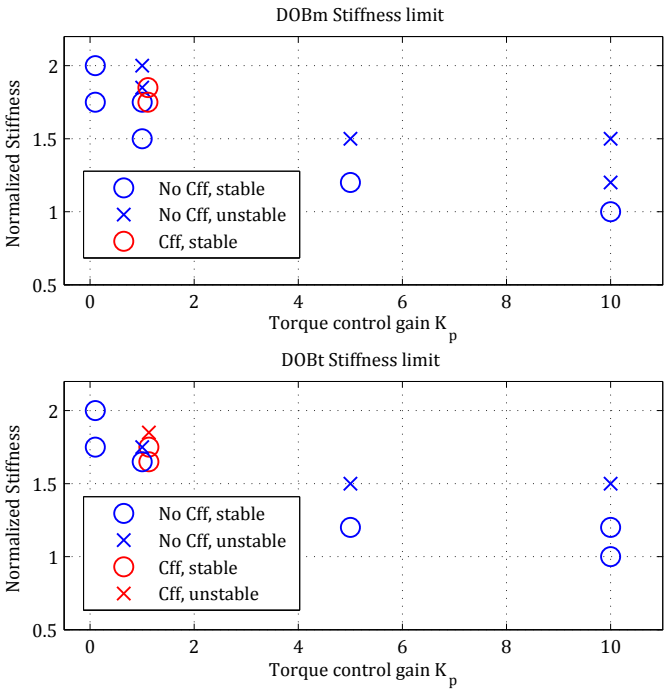

Fig. 7: Normalized stiffness K_{imp}/K vs. K_p, with and without C_{ff}. $K_d = .01$, $B_{imp} = 0$, and $\omega_{DOB} = 25$ Hz for all.

experimental results could be caused by a number of reason such as load side uncertainties, time-delay, or modelling the 3-mass system as a 2-mass.

Further experiments are undertaken to validate the impact of K_p and C_{ff} on the maximum rendered stiffness. In Figure 7, the passive and not passive responses can be seen (x and o, respectively) with and without the C_{ff} from (7). As K_p increases, maximum K_{imp} decreases, although the very low gain ($K_p = .1$) may not render the impedance accurately. The proposed C_{ff} increases the maximum safe stiffness on both the DOBm and DOBt, although the contribution is more minor than suggested analytically.

V. Conclusion

This paper has established initial analysis to the passivity of DOB SEA control, and the DOB's impact on high-stiffness impedance control. Analyzing the load port passivity instead of spring port is important, especially for the DOBt, where the spring port is within the DOB loop and therefore has unusual phase characteristics. It is found that appropriate feedforward control is important for the passivity of the DOB approaches, and it also increases the maximum stiffness they can render experimentally. As the DOB forces the plant to the nominal dynamics, the efficacy of feedforward is improved (the correspondence between the model used in feedforward and plant is improved). With the proposed feedforward compensator, the DOBm achieves a slightly higher maximum safe stiffness than the no DOB case, while the DOBt realizes a slightly lower maximum stiffness. While the DOBt cannot achieve as high of a stiffness, the Z-region is much larger as it reduces the minimum impedance substantially. Both the DOBs offer improved rejection of matched disturbances, such gearbox friction.

The relative importance of control parameters on Z-region and maximum stiffness is also established. The damping term of the impedance controller B_{imp} did not impact the maximum safe stiffness which can be rendered, and was set to 0 to reduce differentiation noise. High gain proportional torque feedback K_p improves the Z-region for the no DOB and DOBm cases, although at very high gains the improvement levels off. Increasing the derivative gain on torque feedback K_d improves Z-region and maximum stiffness monotonically, but is often limited by noise, a topic for future investigation.

References

[1] G. Pratt and M. Williamson, "Series elastic actuators," in *1995 IEEE/RSJ International Conference on Intelligent Robots and Systems 95. 'Human Robot Interaction and Cooperative Robots', Proceedings*, vol. 1, pp. 399–406 vol.1.

[2] N. Hogan, "Impedance control: An approach to manipulation," in *American Control Conference, 1984*. IEEE, pp. 304–313.

[3] K. Ohnishi, M. Shibata, and T. Murakami, "Motion control for advanced mechatronics," vol. 1, no. 1, pp. 56–67.

[4] K. Kong, J. Bae, and M. Tomizuka, "Control of rotary series elastic actuator for ideal force-mode actuation in human–robot interaction applications," vol. 14, no. 1, pp. 105–118.

[5] K. Isik, G. C. Thomas, and L. Sentis, "A Fixed Structure Gain Selection Strategy for High Impedance Series Elastic Actuator Behavior," vol. 141, no. 2.

[6] A. Albu-Schaffer, *et al.*, "Soft robotics," vol. 15, no. 3, pp. 20–30.

[7] K. Haninger and D. Surdilovic, "Bounded Collision Force by the Sobolev Norm: Compliance and Control for Interactive Robots," in *2019 IEEE International Conference on Robotics and Automation (ICRA)*, pp. 8259–8535.
[8] J. E. Colgate and J. M. Brown, "Factors affecting the z-width of a haptic display," in *Robotics and Automation, 1994. Proceedings., 1994 IEEE International Conference On*. IEEE, pp. 3205–3210.
[9] T. Boaventura, *et al.*, "Stability and performance of the compliance controller of the quadruped robot HyQ," in *2013 IEEE/RSJ International Conference on Intelligent Robots and Systems*. IEEE, pp. 1458–1464.
[10] M. Focchi, *et al.*, "Robot Impedance Control and Passivity Analysis with Inner Torque and Velocity Feedback Loops," vol. 14, no. 2, pp. 97–112.
[11] Y. Zhao, *et al.*, "Impedance Control and Performance Measure of Series Elastic Actuators," vol. 65, no. 3, pp. 2817–2827.
[12] H. Vallery, *et al.*, "Passive and accurate torque control of series elastic actuators," in *Intelligent Robots and Systems, 2007. IROS 2007. IEEE/RSJ International Conference On*. IEEE, pp. 3534–3538.
[13] N. L. Tagliamonte and D. Accoto, "Passivity constraints for the impedance control of series elastic actuators," vol. 228, no. 3, pp. 138–153.
[14] F. E. Tosun and V. Patoglu, "Necessary and Sufficient Conditions for Passivity of Velocity-Sourced Impedance Control of Series Elastic Actuators."
[15] M. Mosadeghzad, *et al.*, "Comparison of various active impedance control approaches, modeling, implementation, passivity, stability and trade-offs," in *2012 IEEE/ASME International Conference on Advanced Intelligent Mechatronics (AIM)*, pp. 342–348.
[16] A. Calanca, R. Muradore, and P. Fiorini, "Impedance control of series elastic actuators: Passivity and acceleration-based control," vol. 47, pp. 37–48.
[17] J. E. Colgate and G. G. Schenkel, "Passivity of a class of sampled-data systems: Application to haptic interfaces," vol. 14, no. 1, pp. 37–47.
[18] S. P. Buerger and N. Hogan, "Complementary stability and loop shaping for improved human–robot interaction," vol. 23, no. 2, pp. 232–244.
[19] J. S. Mehling and M. K. O'Malley, "A model matching framework for the synthesis of series elastic actuator impedance control," in *22nd Mediterranean Conference on Control and Automation*. IEEE, pp. 249–254.
[20] H. Lee, *et al.*, "Passivity Analysis of Impedance Controlled Series Elastic Actuators and Design of Time Domain Passivity Observer," p. 8.
[21] K. Haninger and M. Tomizuka, "Robust Passivity and Passivity Relaxation for Impedance Control of Flexible-Joint Robots with Inner-Loop Torque Control," vol. 23, no. 6, pp. 2671–2680.
[22] D. P. Losey, *et al.*, "A Time-Domain Approach to Control of Series Elastic Actuators: Adaptive Torque and Passivity-Based Impedance Control," vol. 21, no. 4, pp. 2085–2096.
[23] J. S. Mehling, J. Holley, and M. K. O'Malley, "Leveraging disturbance observer based torque control for improved impedance rendering with series elastic actuators," in *2015 IEEE/RSJ International Conference on Intelligent Robots and Systems (IROS)*, pp. 1646–1651.
[24] S. Oh and K. Kong, "High-precision robust force control of a series elastic actuator," vol. 22, no. 1, pp. 71–80.
[25] N. Paine, S. Oh, and L. Sentis, "Design and control considerations for high-performance series elastic actuators," vol. 19, no. 3, pp. 1080–1091.
[26] J. Lu, *et al.*, "Design and torque-mode control of a cable-driven rotary series elastic actuator for subject-robot interaction," in *Advanced Intelligent Mechatronics (AIM), 2015 IEEE International Conference On*. IEEE, pp. 158–164.
[27] E. Sariyildiz, G. Chen, and H. Yu, "An acceleration-based robust motion controller design for a novel series elastic actuator," vol. 63, no. 3, pp. 1900–1910.
[28] J. N. Yun, *et al.*, "Robust disturbance observer for two-inertia system," vol. 60, no. 7, pp. 2700–2710.
[29] H. Lee, *et al.*, "Relaxing the Conservatism of Passivity Condition for Impedance Controlled Series Elastic Actuators," p. 6.
[30] K. Haninger, J. Lu, and M. Tomizuka, "Robust Impedance Control with Applications to a Series-Elastic Actuated System," in *Proc. IEEE/RSJ Intl Conf on Intelligent Robots and Systems (IROS)*, pp. 5367–5372.
[31] H. Vallery, *et al.*, "Compliant actuation of rehabilitation robots," vol. 15, no. 3, pp. 60–69.